Materials Science in Semiconductor Processing 201 (2026) 110097

Contents lists available at ScienceDirect

Materials Science in Semiconductor Processing

journal homepage: www.elsevier.com/locate/mssp

Control and tuning of color centers in 4H silicon carbide by application of electric field via Schottky diode☆

Erlend Lemva Ousdal [a,*], Marianne Etzelmüller Bathen [a], Helton Goncalves de Medeiros [b], Augustinas Galeckas [a], Piyush Kumar [b], Maria I.M. Martins [b], Alireza Farzad [a], Andrej Kuznetsov [a], Ulrike Grossner [b], Lasse Vines [a]

[a] Department of Physics/ Centre for Materials Science and Nanotechnology, University of Oslo, 0316 Oslo, Norway
[b] Advanced Power Semiconductor Laboratory, ETH Zürich, Physikstrasse 3, 8092 Zürich, Switzerland

ARTICLE INFO

Keywords:
Silicon carbide
Color center
Quantum defects
Stark effect
Photoluminescence
Semiconductor

ABSTRACT

The ability to tune and manipulate the energy and intensity of photons emitted from color centers in semiconductors is of great importance for developing point defect quantum emitters as a platform for future quantum technology (QT) applications. One of the promising materials to realize point defect based QT is silicon carbide (SiC), as it combines a plethora of color center candidates with mature material processing and device fabrication. Here we explore the use of a Schottky diode, fabricated on a highly doped n-type 4H-SiC epitaxial layer, to control and modulate defect-related emission under both forward and reverse bias conditions. Zero phonon lines (ZPLs) from three prominent color centers are investigated: V1, V1' and V2 assigned to the silicon vacancy, B1 and B2 from the carbon antisite-vacancy pair, and PL4 of the divacancy complex. All the studied defect-related emission wavelengths are found to shift in response to applied bias, but with a varying magnitude and direction of the shift. The electric field-induced variations are assigned to Stark effect and current flow within the device. Furthermore, two unknown defect signatures, labeled K1 and K2, are observed in the vicinity (within 2 meV) of the V2 ZPL and exhibit a strong forward bias dependence. A possible origin related to silicon vacancies perturbed by nearby carbon antisites is discussed.

1. Introduction

Point defect color centers in semiconductors, also known as quantum emitters, are one of several potential platforms to realize quantum technology (QT). Compared to other candidates, color centers offer benefits such as room temperature (RT) single-photon emission and an already existing semiconductor production infrastructure, making technological scaling feasible. The nitrogen-vacancy or NV center in diamond is so far the most widely studied color center in this context, but other more technologically mature materials are rapidly emerging on the scene. Indeed, multiple such color centers have been identified and explored in silicon carbide (SiC), a mature material for power electronics, with the majority of the literature focused on the 4H polytype [1]. 4H-SiC has a wide bandgap of 3.26 eV at RT [2] and exhibits 50% hexagonality, meaning that each atom can be located at either a hexagonal (*h*) or a pseudo-cubic (*k*) lattice site.

Some of the most widely studied point defect single-photon emitters (SPEs) in 4H-SiC include the positively charged carbon antisite-vacancy pair ($C_{Si}V_C$ or CAV), the silicon monovacancy (V_{Si}) in its negative charge state, the neutral silicon-carbon divacancy complex ($V_{Si}V_C$ or VV), and the singly negative nitrogen-vacancy center ($N_{CV,Si}$ or NV) [3–6].

The ZPL from the first optical transition of the V_{Si}^- on a hexagonal lattice site is labeled V1, with V1' being the second excited state of $V_{Si}^-(h)$, while emission from V_{Si}^- on a cubic lattice site is labeled V2 [7]. No second excited state has been observed experimentally for this defect. The divacancy-related ZPLs are labeled as PL1-PL4 corresponding to the *hh*, *kk*, *kh* and *hk* configurations, respectively [8]. Furthermore, there are eight distinct emission lines, labeled the AB-lines, that have been attributed to the CAV complex in 4H-SiC and originate from each of the four possible configurations and their first and second excited states [3]. In this context, A1 and A2 were assigned to the *hh* configuration, A3 and A4 to *hk*, B1 and B2 arise from the *kk* configuration, while the *kh* defect gives rise to the B3 and B4 ZPLs. Odd and even numbers in the label correspond to excited and ground states, respectively [3].

☆ This article is part of a Special issue entitled: 'Quantum defects' published in Materials Science in Semiconductor Processing.

* Corresponding author.
E-mail address: erlendou@uio.no (E.L. Ousdal).

https://doi.org/10.1016/j.mssp.2025.110097
Received 5 June 2025; Received in revised form 8 September 2025; Accepted 24 September 2025
Available online 1 October 2025

The control and manipulation of quantum defects, and in turn photons emitted from them, is important for the progression of semiconductor point defects as a future QT platform. Several approaches for manipulating the emission properties from point defects have been proposed. Among those, dual laser excitation, Schottky diodes, p-i-n diodes and Fermi level control via doping have been employed for defect charge state control, subsequently enabling control over emission intensity [9–13]. Tuning of the emission energy of color centers has also been demonstrated by use of strain, e.g. for the silicon vacancy in diamond [14] and the silicon monovacancy in 6H-SiC microparticles [15]. In addition, the Stark effect, using various device types, has also been shown to be a useful and efficient approach for tuning of emission properties of color centers [10,11,16,17].

One of the most versatile defect control strategies is the introduction of defects into the depletion region of p-i-n diodes and Schottky barrier diodes (SBDs). By subjecting the defects to the electrical field of a diode, it is possible to both control the charge state and induce a Stark shift for the ZPLs of the color center, as demonstrated for V_{Si} and VV in 4H-SiC [10–12]. As a Schottky-diode is easy to produce and control on n-type 4H-SiC, we believe it to be advantageous to study how the color centers behave in this type of device when it is operated under both forward and reverse bias and for different doping conditions, and to extend the previous work to include additional color center types.

This work studies the influence of a Schottky diode under operation on the intensity and wavelength of the emission from color centers in 4H-SiC epitaxial layers. We employ highly doped material with a carrier concentration in the 4H-SiC epitaxial layer of $\sim 1 \times 10^{17}\,cm^{-3}$. This means that the depletion region of the device and thus the expansion of the corresponding electric field is confined to a few 100 nm under zero-bias conditions, in contrast to previous studies employing low-doped SiC epi-layers in the $1 \times 10^{14}\,cm^{-3}$ to $1 \times 10^{15}\,cm^{-3}$ range (see, e.g., Refs. [10,11]), resulting in a more extended field propagation. In addition, we investigate the electric field response of three color centers simultaneously: the silicon vacancy, the divacancy, and the carbon antisite-vacancy pair; the latter has not previously been studied in this context, and an observed Stark shift is reported for this defect. Biasing of the highly doped SiC Schottky diode results in changes in emission properties for all defect types studied herein, including variations in ZPL wavelength and intensity, with the observations depending strongly on the biasing conditions. However, as opposed to previous findings, the observed emission manipulation cannot be explained by a Stark shift induced by the electric field of the depletion region alone, as significant spectral shifts are observed in the forward bias regime. Other effects are probably contributing to the observations, likely related to current propagation through the highly doped device, which is an important factor to control in future device designs, as the demand for isolating a color center from electric charge is highlighted by these findings. This introduces strict requirements for device architectures that reduce electrical charge at interfaces and surfaces, while keeping current flow at a negligible level.

Lastly, we report unidentified PL signatures labeled K1 and K2 that appear after proton irradiation of 4H-SiC which are spectrally located in the vicinity of the V2 ZPL assigned to $V_{Si}^{-}(k)$. K1 and K2 exhibit a similar response to electric fields as V2, but are quenched more rapidly than V2 under forward bias conditions. An origin related to V2, possibly modulated by nearby carbon antisites, is discussed.

2. Methodology

The samples used in this study are 4H-SiC epitaxial layers with a thickness of 10 μm having n-type doping with a carrier density of $1 \times 10^{17}\,cm^{-3}$, as measured by capacitance-voltage, and grown on substrates doped to $8 \times 10^{18}\,cm^{-3}$. The wafer was purchased from CREE/Wolfspeed and diced using a laser cutter to create $4 \times 4\,mm^2$ samples.

Table 1
Estimated width and maximum electric field at RT for a SBD on the sample annealed at 900 °C.

Applied reverse bias (V)	W (μm)	E_{max} ($MVcm^{-1}$)
0	0.3	0.2
50	1.2	0.9
100	1.7	1.2
200	2.3	1.7

To form point defects and defect complexes, the samples were irradiated with 1.8 MeV protons to a fluence of $5 \times 10^{14}\,cm^{-2}$ using a titanium hydride source for the protons. The irradiation process results in a close to uniform distribution of silicon monovacancies in the depletion region, i.e., the concentration of V_{Si} is not responsible for any observed luminescence variation. The distribution is simulated with SRIM [18], using a displacement energy of 20 and 30 eV for C and Si, respectively [10]. The irradiation was followed by annealing in a tube furnace under argon atmosphere for 30 min at the temperatures that generate the strongest defect signature in PL for each complex type. The annealing schemes were chosen based on previous work [19] showing that the highest emission intensities in similar samples were found after annealing at 300 °C for the CAV complex and 900 °C for VV and V_{Si}. In the case of VV, the higher temperature is needed to enable V_{Si} migration and subsequent complex formation, while for V_{Si} and CAV, the signal enhancement is likely caused by a reduction of non-radiative channels, partly related to radiation-induced interstitial defects.

Circular SBDs with a diameter of 900 μm were fabricated on the epi-layer surface by depositing a 100 nm thick layer of Ni through a shadow mask using e-beam evaporation. Prior to Ni deposition, the samples are treated by a full RCA clean to remove surface contamination and oxides. Verification of SBD quality, and determination of carrier concentration after irradiation and annealing, was performed by current–voltage (IV) and capacitance-voltage (CV) measurements. IV and CV measurements were carried out using a Keithley 6487 Picoammeter and a Boonton-7200 high-precision capacitance meter operating at a test frequency of 1 MHz, respectively.

The width of the space charge region (SCR) at different reverse bias for the Schottky diodes on the sample annealed at 900 °C was determined using CV measurements and are listed in Table 1, together with the estimated maximum electric fields in the depletion region, using the expression:

$$E_{\max} = \frac{qN_dW}{\epsilon_s}$$

where q is the elementary charge, N_d is the donor concentration, W is the width of the depletion region and ϵ_s is the permittivity of the semiconductor [20]. It should be noted that these are the widths of the SCR at room temperature and under dark conditions. To support experimental findings, Technology Computer Aided Design (TCAD) simulations of the E-field in the device at RT, with and without a flow of current, are shown in Fig. A.3, with values for the static electric field in the SiC listed in Table A.1. In contrast, the luminescence measurements are done at 10 K. Thus, the depletion region is likely substantially wider during PL measurement due to carrier freeze-out. On the other hand, laser illumination adds energy to the system, ionizing donors, which means that the width of the depletion region probably lies somewhere between that of the non-illuminated sample at 10 K to 300 K.

The built-in potential (V_{bi}) of the diode can be determined from CV measurements by plotting $1/C^2$ against the applied bias, according to the expression

$$\frac{1}{C^2} = \frac{2(V_{bi} - V)}{q\epsilon_s A^2 N_d}$$

where C is the measured capacitance, V is the applied bias and A is the diode area [20]. V_{bi} is then found for $1/C^2 = 0$. The built-in potentials

herein were measured at 2.57 V for the SBD fabricated on the sample annealed at 900 °C, and 1.87 V for the SBD on the reference sample. The sample annealed at 300 °C is found to be heavily compensated due to a high defect density from proton irradiation and limited crystal healing during the low-temperature anneal. As a result, reverse biasing at RT does not change the capacitance of this SBD within the measurement uncertainty, and we are not able to determine the built-in potential of diodes on this sample.

During PL measurements, the sample is cooled down to 10 K and carriers trapped at deep level defects are excited with a laser. Under those conditions, the contacts acts as a Schottky diodes, as also verified by IV-measurements during PL excitation. Thus, the defects are still experiencing the electric field of the SCR and resulting current flow during PL measurement, even in the sample annealed at 300 °C.

The defect emission was studied using an imaging photoluminescence setup with the option of applying bias over the SBDs during the measurements. An illustration of the samples and measurement setup is shown in Fig. 1(a). Photo-excitation is achieved from the backside of the sample at an incident angle of 27 °. Both the laser and the collection lens are focused directly beneath the Schottky contact, with a beam spot of roughly 1 μm depth and 10 μm width, limiting signal from outside the depletion region. In addition, the photocurrent is monitored as a function of the beam focal point, for which we observe photocurrent only when the laser is focused in the SCR. Thus, we assume that most of the observed change in luminescence signal as a function of diode bias is originating from defects within the depletion region of the SBDs.

PL spectroscopy measurements were carried out at 10 K by employing a closed-cycle He refrigerator system and using a 405 nm wavelength cw-laser as an excitation source together with a 550 nm longpass filter. The choice of an off-resonant single 405 nm excitation source is to reduce differences in experimental conditions between samples and defect centers. PL emission was analyzed by an imaging spectroscopy system comprised of a microscope (10x objective, Mitutoyo) coupled to an imaging spectrograph (Horriba Jobin Yvon, iHR320) equipped with an EMCCD camera (Andor, iXon888). In addition, the current through the Schottky diode under study was measured during each photoluminescence measurement. The SciPy library curve_fit was used to fit our data to Lorentzian and Gaussian curves to model the luminescence signatures of the defects.

The TCAD Sentaurus simulation tool from Synopsys was used to investigate the self-heating effect induced by biasing the diodes [21]. An ideal SBD with a Nickel contact and the same 4H-SiC properties as the experimental samples (10 μm epitaxial layer with 1×10^{17} cm^{-3} n-type doping and a substrate with 1×10^{18} cm^{-3} carrier concentration) was simulated. A 2-D meshing was used and the 4H-SiC material properties are taken from a calibrated model [22]. This ideal SBD TCAD model has previously been used to investigate the impact of deep level defects in the SiC bulk on the IV characteristics of SBDs [23]. In this work, we changed the previous SBD TCAD model by including thermal contacts at the top and bottom of the SBD to study the self-heating induced by biasing. We have accounted for the worst-case scenario for self-heating by including a high thermal resistance at both edges of the diode. Simulations were performed for biases ranging from −50 V up to 11 V and temperatures ranging from 150 K up to 300 K. The results for voltages higher than 11 V and below 150 K did not converge, and we have extrapolated the acquired results to those points with a quadratic function.

3. Results & discussion

3.1. Initial defect and device characterization

Fig. 1(b) shows the IV characteristics for the Schottky diodes on a reference sample (in black) and diodes fabricated on the irradiated samples annealed at 300 °C (in red) 900 °C (in blue). Diodes formed on the 300 °C and 900 °C annealed samples were deemed optimal for study of the CAV complex and the V_{Si}/VV defects, respectively. All diodes exhibit a rectifying behavior with a difference of up to four orders of magnitude between ±1 V for the sample annealed at 900 °C, almost three orders of magnitude for the sample annealed at 300 °C, and six orders of magnitude for the reference sample. Interestingly, Fig. 1(b) demonstrates that proton irradiation followed by annealing at 300 °C causes a lowering of both leakage and on-state current for the SBD, while the 900 °C anneal not only remedies that damage, but increases the ON- and OFF-state currents as compared to the pristine (REF.) diode. In other words, Fig. 1(b) demonstrates that both the forward and reverse diode currents are higher in the sample used for measuring V_{Si} and VV (*i.e.*, annealed at 900 °C) as compared to the 300 °C annealed one. The initial as-irradiated defect concentrations in the 300 °C and 900 °C annealed diodes were identical, and only the post-irradiation annealing conditions differ. This indicates a complex interplay between the presence of different defect types and device performance in SiC, and emphasizes the importance of understanding both what defects are present in the device, and how they respond to device operation.

In the following, color center emission wavelength and intensity are found to depend on the various operating conditions of the Schottky diodes under study. Although the bias dependencies of emission properties are related to local electric fields, a possible origin to the observed effects could be the temperature changes due to current-induced heating. In this context, temperature dependent emission of the various color centers of interest in this work was collected, as shown in Fig. 1(c), which demonstrates the temperature dependence of the emission intensity for each ZPL (amplitude relative to the maximum amplitude in the temperature range), and Fig. 1(d), which illustrates the temperature dependence of the ZPL energy (central wavelength or CWL relative to the CWL at 10 K). The intensity of all defect-related emission lines, except for B1 and V1', are found to decrease with increasing temperature for the whole temperature range (see Fig. 1c). It should be noted that the rate of the temperature decrease differs for the B2, V1, V2 and PL4 emission lines, where V2 only decreases by about 20% from 10 – 50 K while PL4 is reduced by almost 80% in the same temperature interval. The decrease in emission intensity is likely caused by an increase in phonon scattering as the temperature increases, resulting in more non-radiative recombination. Thus, temperature will affect defect emission differently, which has to be taken into account when analyzing the bias-dependent data.

Fig. 1(c) further illustrates substantial differences in the optimal measurement temperatures for the color centers B1 and V1', where a temperature activation effect is observed. Indeed, the intensity of the V1' ZPL at 10 K is only 10% compared to the intensity at 40 K, after which point it decreases again. For the B1 peak, the increase is much smaller at around ~10% from 10 K to 20 K. It should, however, be noted that previous reports have shown the intensity of B1 to increase up to a temperature of 40 K after which it stabilizes [24], while our observations show that the intensity increases up to 20 K, after which it slightly decreases. Since the characteristics of CAV is strongly dependent on doping, the observed difference is tentatively attributed to the doping level of the material. Interestingly, both the B1 and V1' emission lines originate from transitions from a second excited state to the ground state of the color center, in contrast to the other ZPLs studied herein. These second excited state transitions (B1 and V1') exhibit so-called negative thermal quenching for the studied temperature range, as opposed to the first excited state transitions (V1, V2, B2 and PL4), which exhibit monotonic thermal quenching. This behavior has previously been discussed as being similar to recombination of excitons bound to ionized-state impurities [25].

Upon comparing the temperature dependent emission energies for the six ZPLs studied herein, we find that all defects exhibit a similar behavior with an overall red shift upon a temperature increase from 10 K to 50 K. This is illustrated as a change in central wavelength (CWL) as a function of temperature in Fig. 1(d). This is likely related to band gap narrowing of the material, making the difference in electronic

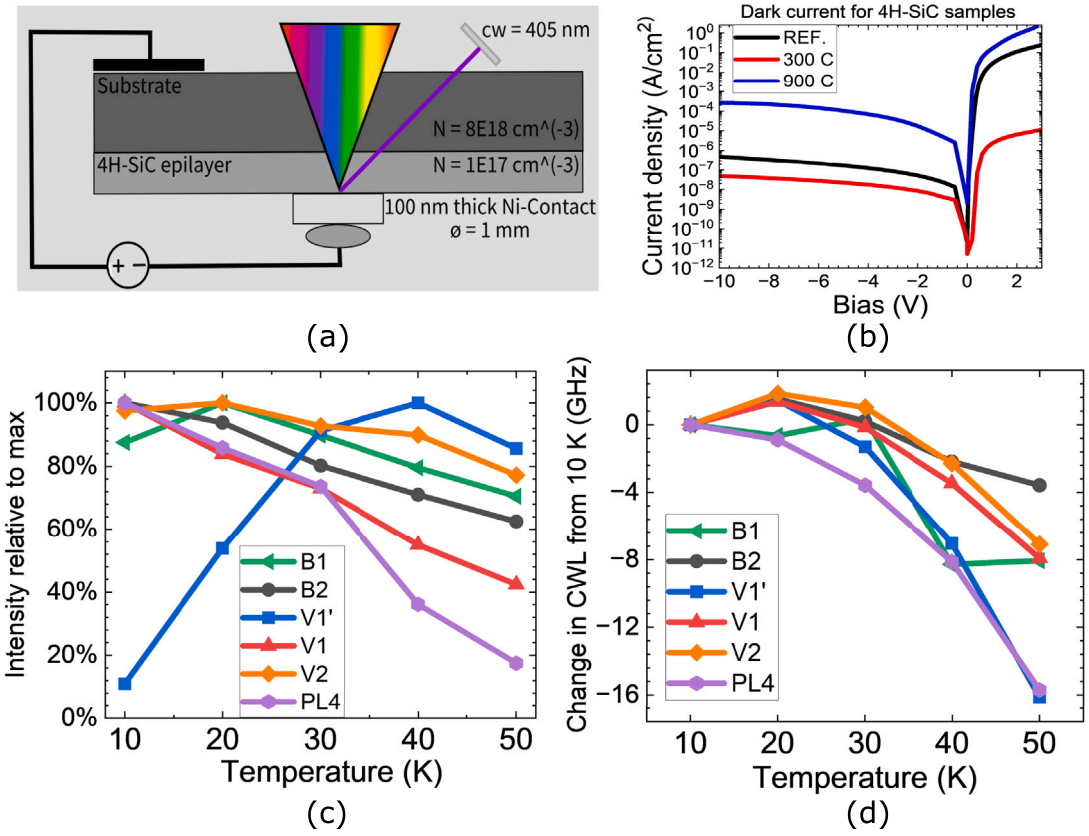

Fig. 1. Initial device and defect characterization. (a) Schematic illustration of the sample details and PL measurement setup used in this work. (b) IV-curves of the Schottky diodes used under dark conditions showing a rectifying diode behavior for both samples annealed under different conditions. (c) Temperature dependence of emission intensity and (d) temperature dependence of central wavelength of the emission lines for all color centers observed in the samples (i.e., B1 and B2 related to CAV, V1', V1 and V2 from the silicon vacancy, and PL4 assigned to the VV).

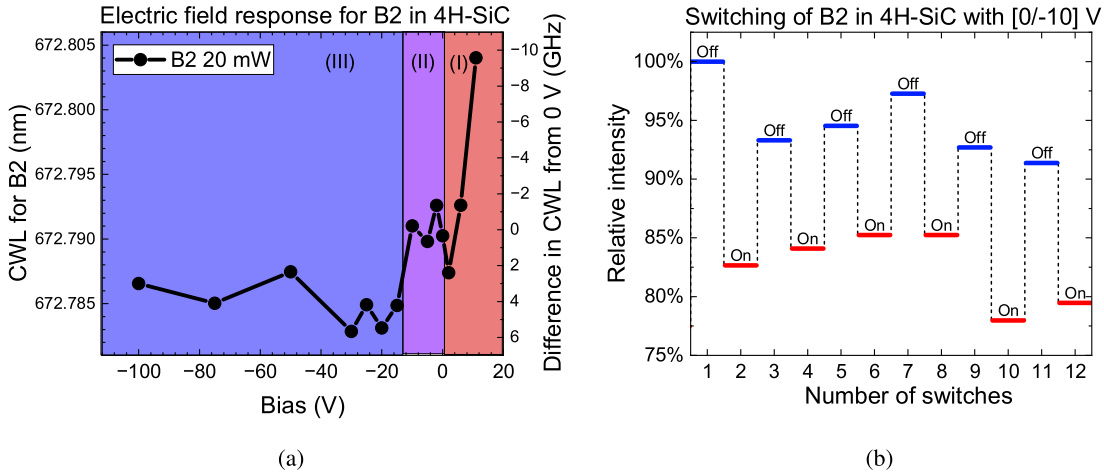

Fig. 2. Electric field response for carbon antisite-vacancy pair. (a) Central wavelength of CAV defects as a function of applied bias for 20 mW laser power (in nm on left y-axis and in GHz on right y-axis). (b) Switching of emission intensity of the B2 line between 0 V and 10 V reverse bias (ON = −10 V, OFF = 0 V). Intensities are given as percentages of the most intense emission.

energy levels smaller. Importantly, the accuracy of the extracted CWL is limited by the quality of the fit of the raw data which depends on the brightness of the color center. An estimate of the quality of the fit is based on the R^2 value of the fit which is found to be 0.78 for the fit of B1, while $R^2 \geq 0.95$ for the fits of all the other signatures.

Interestingly, the magnitude of the CWL change is different when comparing the various color centers. For the B2 line especially, the shift is minor and limited to a few GHz magnitude, while PL4 and V1' display a more prominent shift of the CWL of ~15 GHz.

In the following, the bias dependence of emission will be considered individually for each type of defect. Here we discuss the probable origins for the bias dependency, while also comparing the experimental results to the measured and simulated temperature response of each defect.

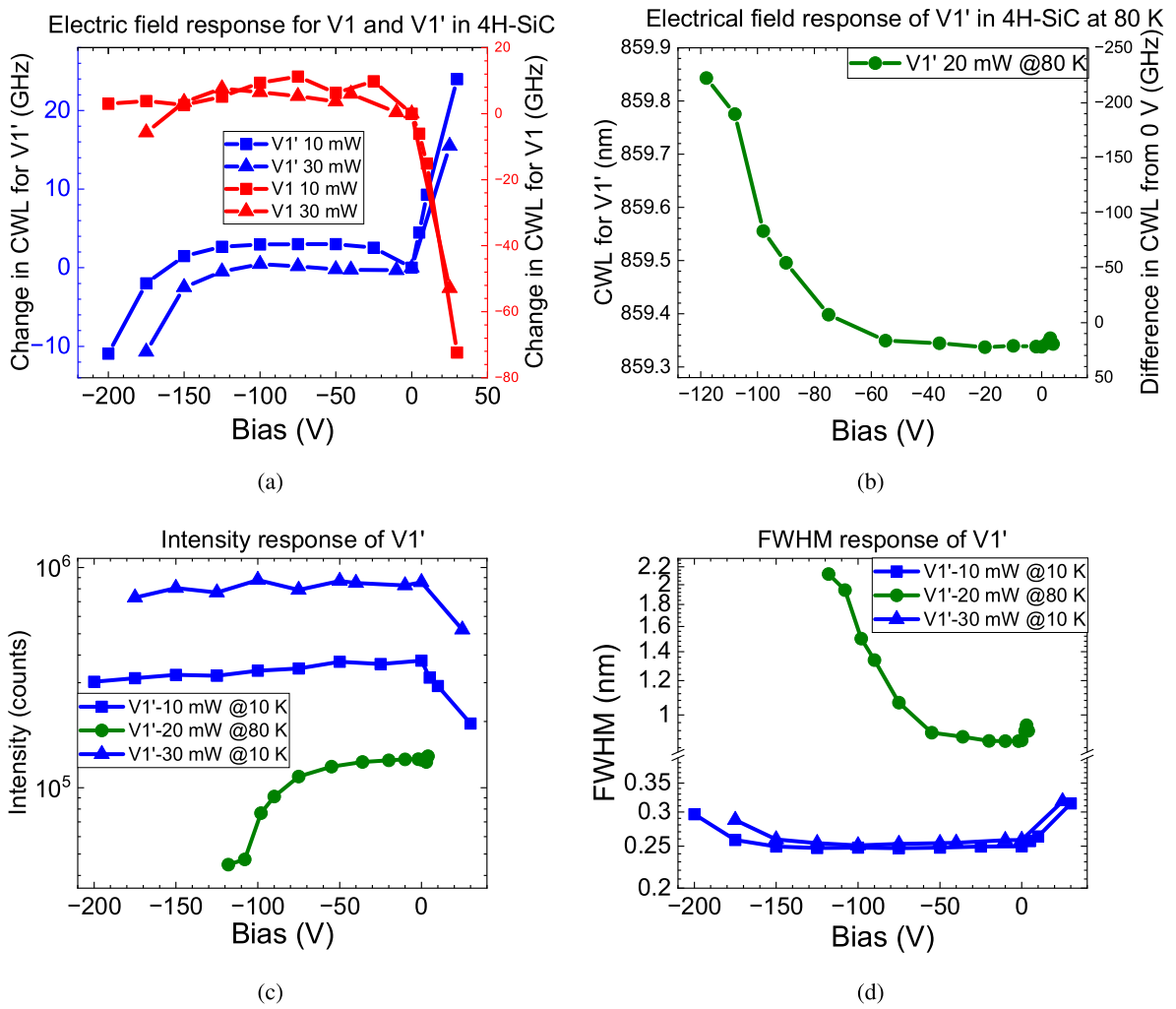

Fig. 3. Electric field response for hexagonal Si vacancy. (a) Electric field response of the central wavelength of the V1 and V1' ZPLs at 10 K for 10 and 30 mW excitation laser. (b) Electric field response of the CWL for the V1' ZPL at 80 K using a 20 mW excitation laser. Panels (c) and (d) show the electric field response of intensity and full width at half maximum, respectively, for V1' at different laser intensities and temperatures.

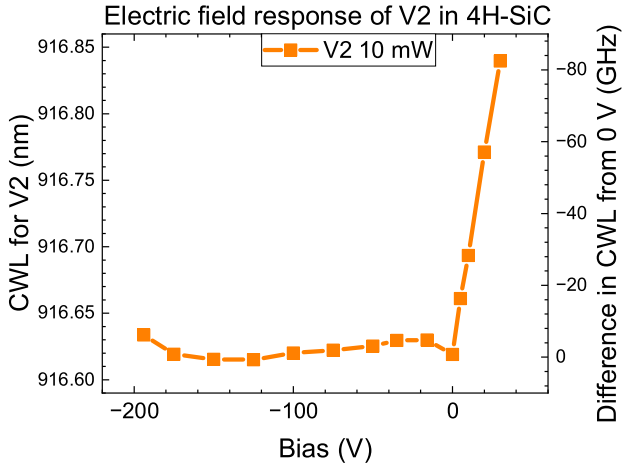

Fig. 4. Electric field response for cubic Si vacancy. Electric field response of the central wavelength of the V2 ZPL at 10 K.

3.2. Carbon antisite-vacancy pair

As mentioned previously, the carbon antisite-vacancy pair or CAV complex can take one of four possible configurations resulting in eight different ZPLs labeled as the AB lines (consisting of the A1-A4 and B1-B4 ZPLs) in the 640 – 680 nm wavelength range. Among these, only B2 and B1 are observed in the samples used herein, which are attributed to the first and second excited state of the *kk*-configuration respectively. Emission intensities of the remaining AB-lines assigned to the CAV complex were below the detection limit in our measurement setup, and are thus not discussed.

First, we consider the electric field response of the CAV pair as presented in Fig. 2, showcasing the response of the B2 ZPL to applied biases in the range −100 V to 11 V. Fig. 2(a), demonstrates the dependence of the central wavelength of the B2 emission line on different biasing conditions. Interestingly, we observe three different types of response: a rapid increase in CWL for increasing forward bias, varying CWL for moderate reverse bias, and a near-constant CWL for larger reverse bias values. The data for B2 is therefore divided into three regions in Fig. 2(a): (I) forward bias in red, (II) moderate reverse bias in the range 0 V to −20 V in purple, and (III) stronger reverse bias in the range of −20 V to −100 V in blue. In region I (red shaded area of Fig. 2a), there is a rapid decrease in the emission energy of B2 with increasing forward bias. Region II with a moderate reverse bias of 0 V to −15 V (purple shaded area of Fig. 2a) is termed a "metastable" region herein as the

B2 ZPL energy first diminishes, until it is increasing again in region III (blue shaded area of Fig. 2a). This suggests that there are competing mechanisms that control the emission energy shift in regions II and III, where the mechanism responsible for the behavior observed in region III becomes dominant above a reverse bias threshold voltage of ~18 V.

In forward bias (region I), where the largest CWL shift is observed in Fig. 2(a), the large ON-state current can induce a temperature increase. Indeed, the direction of the shift of the B2 emission energy (towards lower energy) is consistent with what is expected from an increase in temperature according to Fig. 1(d). However, under 10 V forward bias the ZPL shift is ~12 GHz, while only a ~4 GHz shift was found for B2 when increasing the temperature from 10 K to 50 K (see Fig. 1d). Thus, the forward bias-induced shift of the B2 CWL exceeds that which can be expected based on a current-induced temperature increase alone. Indeed, supporting TCAD simulations indicate that the maximum temperature increase that can be caused by current-induced heating under the relevant measurement conditions is below 2 K, see Fig. A.1 in the Appendix for further details. Instead, the current flow through the device is a possible source of the ZPL energy variations. In the case of the regions II and III, the CWL shift varies in magnitude. A possible mechanism here is the Stark effect, as observed for the V_{Si} and VV in previous studies [10,11,17], confirming that we are probing defects in the SCR. However, the variation is so small that we cannot confidently discard the effects of random variations in the material, as variations due to color centers outside of the very narrow depletion region is also contributing to the total signal, although less than the defects within the SCR. The difference between regions II and III could thus be explained by an expansion of the depletion region to a width at which all the measured signal originates from color centers in the SCR. If this was the case, we would expect a narrowing of FWHM under reverse bias as the probed region became more homogeneous, however we do not observe any significant change in the FWHM for the whole range of bias that is used for shifting of CAV herein, as shown in Figure A4. As such, both a static Stark effect caused by the depletion region and a dynamic response due to local electric fields induced by charge accumulation under forward bias may come into play.

The intensity of the emission from the B2 ZPL assigned to the CAV complex can be toggled with repeated sequences of applied reverse bias as shown in Fig. 2(b), causing a sequential quenching of B2 emission intensity. Here, OFF designates 0 V applied bias while ON refers to an applied reverse bias of −10 V. Intensities are given as percentages of the most intense emission, i.e., cycle nr. 1. The largest change in emission intensity occurs in the first switching and results in a reduction of about 17%. Operating the diode on the sample annealed at 300 °C at 0 and −10 V results in little or no current, in the order of magnitude of 1×10^{-8} A/cm^2, as seen in Fig. 1(b), and we do not expect current-induced effects to have an impact on intensity switching. Instead, we tentatively attribute the switching mechanism to band bending, leading to a change in the predominant charge state of the CAV complex. The singly positive charge state is optically active and gives rise to the AB lines, while both the neutral and double negatively charged CAV complexes are assumed to be dark. Such a band-bending effect causing emission intensity control was previously demonstrated for the V_{Si} [10] in Schottky diodes and the VV in p-i-n diodes [11]. By applying a reverse bias to the Schottky diode, the Fermi level shifts relative to the charge transition levels of the defect. For the $C_{Si}V_C^+$, theoretical work based on density functional theory (DFT) calculations and TCAD simulations predicted that the region where the bright charge state is stable shifts away from the surface with increasing reverse bias [26]. This is in agreement with our observations, where the intensity of the B2 line decreases for applied reverse bias, when the laser is focused within the depletion region of the Schottky diode.

It should be noted that there is some variation in the absolute intensities of the OFF and ON states of the B2 ZPL which is attributed to variations in the defect environment that complicates distinguishing between ON- and OFF-states for a single-cycle measurement. There is some observed variation in the reported switching of V_{Si} and VV [10,11], and the observed variations herein is similar or slightly higher, which can be attributed to contributions from defects outside the SCR.

3.3. Silicon monovacancies

The silicon vacancy in different lattice configurations has been attributed to three different ZPLs in 4H-SiC: V1' at 858 nm assigned to the second excited state of $V_{Si}^-(h)$, V1 at 861 nm arising from the first excited state of $V_{Si}^-(h)$, and V2 at 916 nm attributed to the first (and only) excited state of $V_{Si}^-(k)$. The optical transition dipoles of V1/V2 and V1' are orthogonally polarized to each other, which makes it challenging to extract a strong signal from both defect states at the same time [7,27]. In this work, the optical excitation is mostly parallel to the c-axis ⟨0001⟩ which favors emission from the V1' ZPL. However, as the sample is excited at an incident angle of 27 ° (see Fig. 1a), there is still a visible emission signal from defects that have transition dipoles polarization parallel to the c-axis (*e.g.*, V1 and V2) [7,27].

Fig. 3 shows the biasing response of $V_{Si}^-(h)$ including CWL response at 10 K (Fig. 3a) and 80 K (Fig. 3b), intensity response of V1' (Fig. 3c), and full width half maximum (FWHM) response of V1' (Fig. 3d). The most notable outcome of the biasing study of $V_{Si}^-(h)$ is the impact of forward biasing the sample on the V1 and V1' ZPLs (Fig. 3a). During forward bias, V1' exhibits a distinct blue shift. V1, on the other hand, shows a red shift under forward bias. The same trend (red shift under forward bias) is found for the central wavelength of the V2 ZPL, see Fig. 4. In contrast, a temperature increase from 10 K causes the same behavior for V1, V1' and V2: a small blue shift at 20 K followed by a consistent red shift (see Fig. 1d). Interestingly, this excludes the possibility that the shift in ZPL energy for all three defect emission lines in the forward direction occurs as a result of ohmic heating. Although a heating-induced red shift in theory could explain the red shift for the V1 and V2 ZPLs, a CWL shift of this magnitude would require a current-induced temperature increase of more than 100 K, as extrapolated from Fig. 1(d). From our TCAD simulations, there should be almost no temperature increase under our forward biasing conditions for temperatures lower than 135 K. Instead, it is possible that the shifts observed under forward bias are caused by local electrical fields induced by mobile injected carriers. This is further supported by the fact that the direction of the shift of V1', which has an optical dipole orientation parallel to the direction of current, is dependent on the direction of the current flow, as a red shift is observed for V1' for large enough reverse biases that the current increases (> 150 V reverse bias).

The energies of all three emission lines from the silicon monovacancies are relatively stable as a function of reverse bias from 0 V to around −150 V. This is in contrast to previous reports, in which a linear Stark shift is observed for both V1 and V2 [28–30]. The lack of Stark effect under reverse bias is tentatively attributed to the screening of the electric field in the SCR by either interface-charges or the accumulation of photo-generated charge carriers, an effect that is less pronounced in wider depletion regions such as those reported previously in the literature. The forward bias response is attributed to a combination of defects both close to the metal–semiconductor interface and deeper in the SiC bulk. As such, Ohmic contacts may yield similar forward-bias responses, but this requires further investigation. At reverse bias higher than 150 V, the V1' ZPL exhibits a significant shift of approximately 10 GHz when increasing the reverse bias, (Fig. 3a), while both V1 and V2 remain stable within the spectrometer precision limit of ± 0.075 nm (Figs. 3(a) and 4). This indicates that V1', the second excited state transition of $V_{Si}^-(h)$, is more responsive to an applied electric field than the monovacancy's first excited states. This is also corroborated by higher-temperature measurements of V1' at 80 K, as shown in Fig. 3(b). The measurements reveal that the magnitude of the CWL shift for V1' under reverse bias increases substantially at 80 K compared to 10 K, and that the applied bias required to produce a CWL shift for V1' is reduced at the higher temperature. It could be speculated that this is due to V1' having a polaronic character rather than being purely electronic, as the electron–phonon coupling is more pronounced [31]. Importantly, the reverse bias at which the shift onset occurs is correlated with

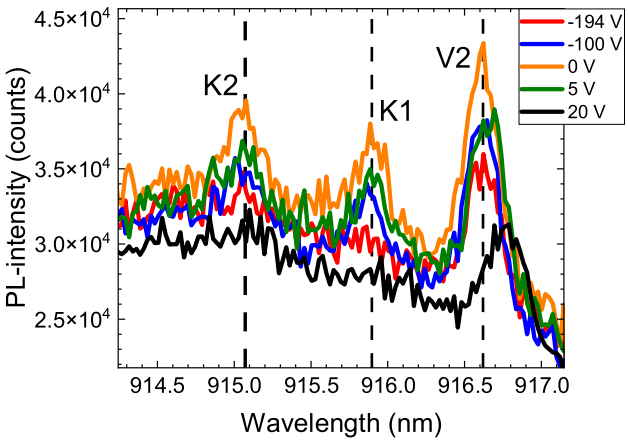

Fig. 5. PL spectra showing the K1 and K2 peaks close to the V2 signature collected for 20 V, 5 V, 0 V, −100 V and −194 V applied bias. Measurements are done at 10 K, using a laser power of 10 mW.

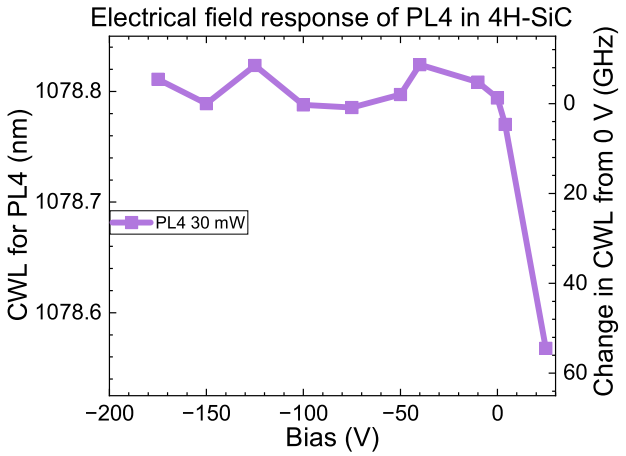

Fig. 6. Shift in central wavelength of emission as a function of applied bias for the PL4 ZPL in 4H-SiC with 30 mW excitation laser at 10 K.

the reverse bias leakage current of the Schottky diode at both 10 K and 80 K. This red shift is tentatively attributed to the accumulation of injected charge carriers inducing local electric fields. As for the response to forward bias, we were not able to supply more than 3 V due to the current limitations of the power supply. It should, however, be noted that even though the device is operated outside of equilibrium due to the generation of charge carriers from photoexcitation, there is a difference in the level of freeze-out due to the thermal energy. As such, a difference in the electric field in the SCR between the two temperatures may arise, which may also contribute to the observed difference in bias response.

To further understand the response of the V1' ZPL to the electric field imposed by the Schottky diode, we compare the bias dependency of the intensity and FWHM at both 10 K and 80 K and for different excitation powers. See Figs. 3(c) and 3(d) for intensity and FWHM response, respectively. The figures reveal a relation between the intensity and FWHM of the V1' emission, as higher temperature corresponds to a larger FWHM and lower intensity, suggesting an increase in phonon-assisted recombination through non-radiative pathways, which is more pronounced at 80 K than at 10 K. Interestingly, the FWHM and intensity seem to be correlated with the CWL-shift, suggesting that they are all probing the same effect. Note that the dependence of intensity and FWHM on bias could not be accurately determined for the V1 or V2 ZPLs on account of low count rates due to the orientation of the sample relative to the excitation laser, leading to large uncertainties, and is therefore not shown herein.

Interestingly, the PL emission in the spectral range near the V2 ZPL exhibits additional sharp features, as shown in Fig. 5. These two peaks, labeled K1 and K2 herein, appear in the PL spectrum of the sample annealed at 300 °C and with a spectral distance from V2 of 1.0 meV and 2.2 meV, respectively. The K-peaks behave similarly to V2 with respect to applied voltage (see Fig. 5), both in terms of CWL shift and intensity change, prompting the speculation that they are related to V2. However, when the samples are forward biased above a threshold voltage, the intensity of the K-peaks are reduced below the detection limit, but this is not the case for V2. For this sample, the voltage at which the K-peaks disappear is at around 10 V in the forward direction. Reducing the bias below this threshold voltage returns the signal of both the K-peaks, thus the effect of high forward biasing is reversible.

A similar set of neighboring peaks were previously found near the V1 and V1' ZPLs, which are attributed to a pseudo Jahn-Teller effect [25]. More recently, an alternative model was proposed for these peaks, relating them to perturbation of the silicon vacancy by a nearby carbon antisite in close proximity [32]. This is also a possible model for the K1 and K2 peaks — *i.e.*, that they originate from a silicon vacancy at a cubic lattice site that is perturbed by one or more nearby carbon antisites. Based on theoretical predictions [32], K1 may originate from a V_{Si} being perturbed by a C_{Si} in the plane directly above the V_{Si}, *i.e.*, along the *c*-axis. K2 would according to the model originate from a V_{Si} that is perturbed by a C_{Si} three planes below along the *c*-axis. In this case, the quenching of the PL signal from K1 and K2 may be caused by a reduced interaction between V_{Si} and the mentioned C_{Si} as forward bias, and current, increases, suggesting that the perturbation range of the carbon antisites is lowered as the current increases. Alternatively, the earlier quenching of the K-peaks as compared to V2 may be related to the differing signal intensities and the detection limit of the PL setup. Regardless, the response of the K-lines to an applied electric field strengthens the claim that they are related to V2. The quenching of the PL signal from the K-peaks at forward bias also provides a possible pathway to eliminate the PL-signal from the K-signatures and isolate the V2 signature.

3.4. Divacancy complex

The divacancy complex can be found in four different configurations in 4H-SiC, giving rise to four ZPLs labeled PL1-4 (and sometimes UD-lines). In this work we have focused on the PL4 line, which is attributed to the *hk* configuration of the divacancy [8], as it is the brightest emission line from the VV-defect in our measurements. The response of PL4 to an electric field can be seen in Fig. 6. While there is some variation between individual biases, there is overall only minor, non-significant, changes in the PL4 ZPL energy between 0 V and −175 V applied reverse bias. Interestingly, previous work using a PIN-diode to manipulate VV emission found Stark shifts of several hundred GHz in the same bias regime [11]. Although an unambiguous explanation for the observed difference is lacking, it is likely related to the use of different device architectures and the doping concentration of the semiconductor material.

When subjected to forward bias, the PL4 ZPL exhibits a strong blue shift approaching 60 GHz in magnitude (Fig. 6). This is similar to that which is observed for V1', whereas both the B2, V1 and V2 ZPLs are red shifted when subjected to a forward bias. Interestingly, PL4 and V1' also exhibit stronger temperature responses than the other color centers studied herein (see Fig. 1d). This suggests that one should have observed the largest red shift for PL4 and V1' as compared to the other color centers if the effect had been temperature-induced, however, the opposite is observed. It should however be noted that the intensity of PL4 is strongly quenched under forward bias, as predicted by the temperature dependency of Fig. 1(c). The direction of the shift

could be related to the polarization-axis of emitted photons from both V1' and PL4, as they are both parallel to the c-axis, and the shifting mechanism is attributed to local electric fields induced by injected charge carriers [33].

4. Concluding remarks

We study the response to external perturbation of three color center ensembles in 4H-SiC: the carbon antisite-vacancy pair, the silicon vacancy, and the divacancy. The impact of temperature, device fabrication and Schottky diode biasing is considered for each defect type. In particular, the color centers' response to an applied electric field is mapped out. Photon energy control of tens to hundreds of GHz is achieved. This corroborates previous reports that Schottky diode biasing is a viable avenue for controlling defect emission for the V_{Si} and VV defect centers. Such fine-tuning of emission energies can be important in the generation of creating indistinguishable photons. Electric field control has been shown for V_{Si} and VV previously, but is herein demonstrated for the CAV complex as well.

The color center emission is found to strongly depend on both the electrical device fabrication and its dynamic operating conditions. The highly doped epitaxial layers employed herein exhibit high current in forward and leakage regimes, which we believe can cause local electrical fields from the accumulation of charge carriers, as also simulated by TCAD (not shown). This is found to impact the color centers differently from previous studies on low-doped Schottky and p-i-n diodes. However, it should be noted that because the flow of current is thought to contribute to the observed effects, it is likely that ohmic contacts can achieve the same results, while Schottky contacts are needed for limiting current-related effects. Moreover, the response of the color center emission wavelengths to applied bias is found to increase as the temperature of the sample goes from 10 K to liquid-nitrogen temperatures (80 K). This is interesting in terms of future technological development where higher temperatures are beneficial.

Finally, we observe a set of unknown peaks in the vicinity of the V2 ZPL assigned to the $VSi^{-}(k)$, labeled K1 and K2 and situated 1.0 meV and 2.2 meV away from V2, respectively. Comparison to theoretical predictions suggests a possible model for the K-peaks as related to Si vacancies that are modified by nearby carbon antisites.

CRediT authorship contribution statement

Erlend Lemva Ousdal: Writing – review & editing, Writing – original draft, Visualization, Validation, Software, Project administration, Methodology, Investigation, Formal analysis, Data curation, Conceptualization. **Marianne Etzelmüller Bathen:** Writing – review & editing, Validation, Supervision, Resources, Project administration, Methodology, Investigation, Funding acquisition, Formal analysis, Conceptualization. **Helton Goncalves de Medeiros:** Writing – review & editing, Visualization, Validation, Software, Methodology, Investigation, Formal analysis, Data curation. **Augustinas Galeckas:** Writing – review & editing, Validation, Resources, Methodology, Data curation. **Piyush Kumar:** Resources, Methodology. **Maria I.M. Martins:** Resources, Methodology, Data curation. **Alireza Farzad:** Investigation, Formal analysis, Data curation. **Andrej Kuznetsov:** Supervision, Project administration, Funding acquisition. **Ulrike Grossner:** Project administration, Investigation, Funding acquisition, Formal analysis, Conceptualization. **Lasse Vines:** Writing – review & editing, Validation, Supervision, Resources, Project administration, Methodology, Investigation, Funding acquisition, Formal analysis, Conceptualization.

Declaration of competing interest

The authors declare that they have no known competing financial interests or personal relationships that could have appeared to influence the work reported in this paper.

Acknowledgments

Financial support was kindly provided by the Research Council of Norway, Norway and the University of Oslo through the research project QuTe (no. 325573) and the Norwegian Micro- and Nano-Fabrication Facility, NorFab, project number 295864. The authors gratefully acknowledge Axel Erlenbach for his valuable discussions regarding the TCAD-related work.

Appendix

The results in Fig. A.1(a) illustrate the simulated change in temperature (ΔT) induced in the silicon carbide epitaxial layer for different biasing and simulation temperature conditions. Simulations for biases above 11 V and for temperature lower than 150 K did not converge and are not shown in Fig. A.1(a). In order to estimate the ΔT at the relevant operation point (10 K and 30 V), we have extrapolated the simulated data to those operation points, see Fig. A.1(b). Note that the ΔT listed in Fig. A.1 is the maximum induced temperature change within the entire 4H-SiC epi-layer, and not the average induced temperature in the material.

Fig. A.2 show the results from SRIM-simulations of implantation of 1.8 MeV H^{+}, which is the same implantation that is used to generate

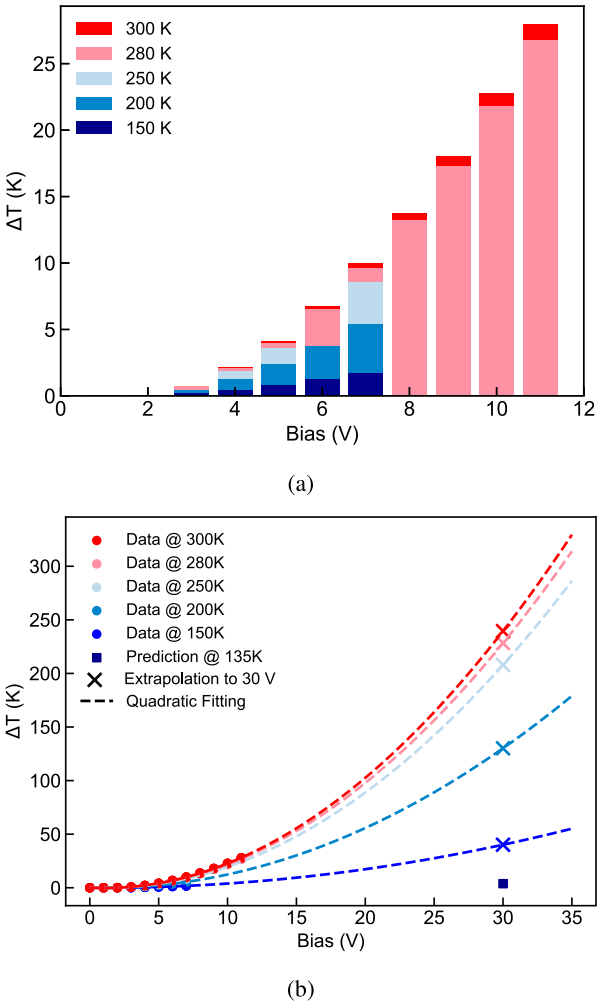

Fig. A.1. TCAD simulations dependent on applied bias and temperature. (a) Simulated datapoints in TCAD, notice that the −50 V data point is not shown because the ΔT is zero. (b) The quadratic extrapolation both to 30 V and to 135 K are shown.

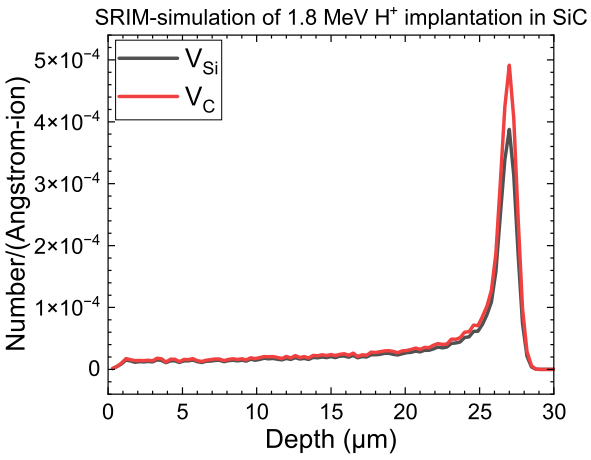

Fig. A.2. Simulated vacancy distribution after implantation of 1.8 MeV H^+ using displacement energies of 20 eV and 30 eV for C and Si respectively [10]. The simulations are performed in SRIM-2008 [18].

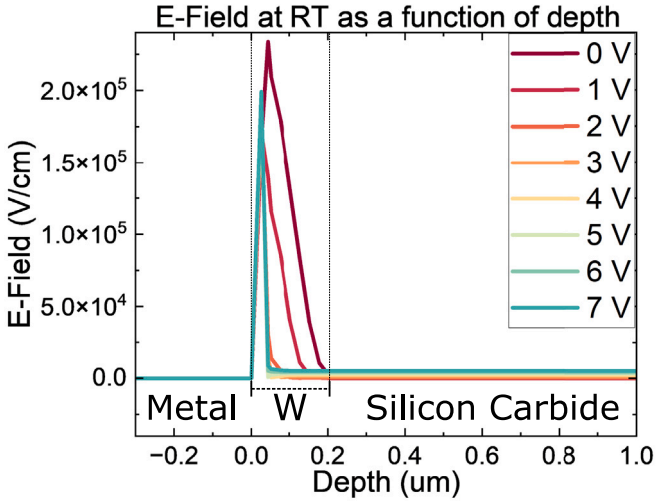

Fig. A.3. TCAD simulations of the electric field distribution in the device under forward biasing, with a depth of 0 μm being referenced to the metal–semiconductor interface. The simulations use a free carrier concentration in SiC of 1×10^{17} cm^3.

vacancies in this study. The resulting vacancy distribution is shown as a function of depth, which shows that the vacancy concentration is relatively stable up to about 25 μm. It is therefore expected that the concentration of V_{Si} is homogeneous in the probing volume in the depletion region of the Schottky diode.

Simulation results of the E-field in the device at RT are shown in Fig. A.3, and the static E-field in the SiC as a function of forward bias is listed in Table A.1. From the figure, the E-field in the depletion region is much higher than in the rest of the device, while the E-field in the semiconductor outside of the depletion region is increasing as a function of the forward bias. The width of the depletion region decreases as the forward bias is increased, in accordance with the ideal diode equation.

Fig. A.4 shows the FWHM of B2 as a function of applied bias. There is no observable trend to shift in the measured FWHM, suggesting that the measured environment is stable and does not contain fluctuating fields.

Table A.1
Electric field in SiC as a function of forward bias applied to the Schottky diode.

Bias (V)	E-field (V/cm)
0	0
1	1.12E−15
2	411
3	1390
4	2391
5	3382
6	4387
7	5395

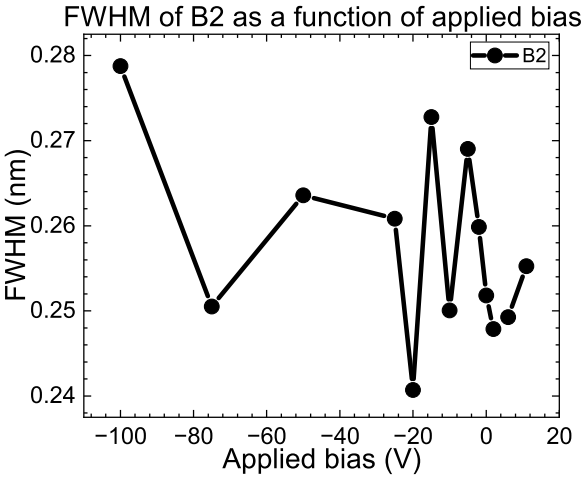

Fig. A.4. Showing FWHM of B2 as a function of applied bias.

Data availability

Data will be made available on request.

References

[1] S. Castelletto, L. Rosa, B.C. Johnson, Silicon carbide for novel quantum technology devices, in: Advanced Silicon Carbide Devices and Processing InTech, 2015.
[2] C. Haberstroh, R. Helbig, R.A. Stein, Some new features of the photoluminescence of SiC(6H), SiC(4H), and SiC(15r), J. Appl. Phys. 76 (1994) 509–513.
[3] S. Castelletto, B.C. Johnson, V. Ivády, N. Stavrias, T. Umeda, A. Gali, T. Ohshima, A silicon carbide room-temperature single-photon source, Nat. Mater. 13 (2014) 151–156.
[4] M. Widmann, S.-Y. Lee, T. Rendler, N.T. Son, H. Fedder, S. Paik, L.-P. Yang, N. Zhao, S. Yang, I. Booker, A. Denisenko, M. Jamali, S.A. Momenzadeh, I. Gerhardt, T. Ohshima, A. Gali, J. Janzén, E. and Wrachtrup, Coherent control of single spins in silicon carbide at room temperature, Nat. Mater. 14 (2015) 164–168.
[5] D.J. Christle, A.L. Falk, P. Andrich, P.V. Klimov, J. Ul Hassan, N.T. Son, E. Janzén, T. Oshima, D.D. Awschalom, Isolated electron spins in silicon carbide with millisecond coherence times, Nat. Mater. 14 (2015) 160–163.
[6] Z. Mu, S.A. Zargaleh, H.J. von Bardeleben, J.E. Fröch, M. Nonahal, H. Cai, X. Yang, J. Yang, X. Li, I. Aharonovich, W. Gao, Coherent manipulation with resonant excitation and single emitter creation of nitrogen vacancy centers in 4H silicon carbide, Nano Lett. 20 (2020) 6142–6147.
[7] E. Janzén, A. Gali, P. Carlsson, A. Gällström, B. Magnusson, N. Son, The silicon vacancy in SiC, Phys. B: Condens. Matter 404 (2009) 4354–4358.
[8] J. Davidsson, V. Ivády, R. Armiento, N.T. Son, A. Gali, I.A. Abrikosov, First principles predictions of magneto-optical data for semiconductor point defect identification: the case of divacancy defects in 4H-SiC, New J. Phys. 20 (2018) 023–035.
[9] G. Wolfowicz, C.P. Anderson, A.L. Yeats, S.J. Whiteley, J. Niklas, O.G. Poluektov, F.J. Heremans, D.D. Awschalom, Optical charge state control of spin defects in 4H-SiC, Nat. Commun. 8 (2017) 1876.
[10] M.E. Bathen, A. Galeckas, J. Müting, H.M. Ayedh, U. Grossner, J. Coutinho, Y.K. Frodason, L. Vines, Electrical charge state identification and control for the silicon vacancy in 4H-SiC, Npj Quantum Inf. 5 (2019) 111.

[11] C.P. Anderson, A. Bourassa, K.C. Miao, G. Wolfowicz, P.J. Mintun, A.L. Crook, H. Abe, J.U. Hassan, N.T. Son, T. Ohshima, D.D. Awschalom, Electrical and optical control of single spins integrated in scalable semiconductor devices, Science 366 (2019) 1225–1230.
[12] M. Widmann, M. Niethammer, D.Y. Fedyanin, I.A. Khramtsov, T. Rendler, I.D. Booker, J. Ul Hassan, N. Morioka, Y.-C. Chen, I.G. Ivanov, N.T. Son, T. Ohshima, M. Bockstedte, A. Gali, C. Bonato, S.-Y. Lee, J. Wrachtrup, Electrical charge state manipulation of single silicon vacancies in a silicon carbide quantum optoelectronic device, Nano Lett. 19 (2019) 7173–7180.
[13] N.T. Son, I.G. Ivanov, Charge state control of the silicon vacancy and divacancy in silicon carbide, J. Appl. Phys. 129 (2021) 215702.
[14] S. Meesala, Y.-I. Sohn, B. Pingault, L. Shao, H.A. Atikian, J. Holzgrafe, M. Gündoğan, C. Stavrakas, A. Sipahigil, C. Chia, R. Evans, M.J. Burek, M. Zhang, L. Wu, J.L. Pacheco, J. Abraham, E. Bielejec, M.D. Lukin, M. Atatüre, M. Lončar, Strain engineering of the silicon-vacancy center in diamond, Phys. Rev. B 97 (2018) 205444.
[15] G.C. Vásquez, M.E. Bathen, A. Galeckas, C. Bazioti, K.M. Johansen, D. Maestre, A. Cremades, Ø. Prytz, A.M. Moe, A.Y. Kuznetsov, L. Vines, Strain modulation of si vacancy emission from sic micro- and nanoparticles, Nano Lett. 20 (2020) 8689–8695, pMID: 33175553.
[16] C.F. de las Casas, D.J. Christle, J. Ul Hassan, T. Ohshima, N.T. Son, D.D. Awschalom, Stark tuning and electrical charge state control of single divacancies in silicon carbide, Appl. Phys. Lett. 111 (2017) 262403.
[17] M. Rühl, L. Bergmann, M. Krieger, H.B. Weber, Stark tuning of the silicon vacancy in silicon carbide, Nano Lett. 20 (2020) 658–663, pMID: 31809057.
[18] J.F. Ziegler, M. Ziegler, J. Biersack, SRIM - the stopping and range of ions in matter (2010), Nucl. Instrum. Methods Phys. Res. Sect. B: Beam Interactions Mater. Atoms 268 (2010) 1818–1823, 19th International Conference on Ion Beam Analysis.
[19] E. Lemva Ousdal, M. Etzelmuller Bathen, A. Galeckas, A. Kuznetsov, L. Vines, Formation and stability of point defect color centers in 6h silicon carbide, J. Appl. Phys. 135 (2024) 225701.
[20] B.G. Streetman, S. Banerjee, Solid State Electronic Devices, seventh ed., Pearson, Boston, 2014.
[21] Mountain View, CA, USA, Sentaurus TCAD documentation (version 2020.09), 2020.
[22] A. Tsibizov, I. Kovačević-Badstübner, B. Kakarla, U. Grossner, Accurate temperature estimation of sic power mosfets under extreme operating conditions, IEEE Trans. Power Electron. 35 (2019).
[23] H. G. Medeiros, A.K. Brandl, P. Kumar, H. Scriba, S. Vuillemin, S. Race, I. Kovačević-Badstübner, M.E. Bathen, U. Grossner, On how to implement experimentally obtained defect characteristics in sic device simulation, in: 2025 IEEE International Reliability Physics Symposium, IRPS, 2025, pp. 01–06.
[24] J.W. Steeds, Photoluminescence study of the carbon antisite-vacancy pair in 4H- and 6H-SiC, Phys. Rev. B 80 (2009) 245202.
[25] M.E. Bathen, A. Galeckas, R. Karsthof, A. Delteil, V. Sallet, A.Y. Kuznetsov, L. Vines, Resolving jahn-teller induced vibronic fine structure of silicon vacancy quantum emission in silicon carbide, Phys. Rev. B 104 (2021) 045120.
[26] M.E. Bathen, G.M. Selnesaunet, M.J. Enga, S.B. Kjeldby, J. Müting, L. Vines, U. Grossner, Charge state control over point defects in sic devices, Defect Diffus. Forum 425 (2023) 35–42.
[27] R. Nagy, M. Widmann, M. Niethammer, D.B.R. Dasari, I. Gerhardt, O.O. Soykal, M. Radulaski, T. Ohshima, J. Vučković, N.T. Son, I.G. Ivanov, S.E. Economou, C. Bonato, S.-Y. Lee, J. Wrachtrup, Quantum properties of dichroic silicon vacancies in silicon carbide, Phys. Rev. Appl. 9 (2018) 034022.
[28] D.M. Lukin, A.D. White, R. Trivedi, M.A. Guidry, N. Morioka, C. Babin, Ö.O. Soykal, J. Ul-Hassan, N.T. Son, T. Ohshima, P.K. Vasireddy, M.H. Nasr, S. Sun, J.-P.W. MacLean, C. Dory, E.A. Nanni, J. Wrachtrup, F. Kaiser, J. Vučković, Spectrally reconfigurable quantum emitters enabled by optimized fast modulation, Npj Quantum Inf. 6 (2020) 80.
[29] T. Steidl, P. Kuna, E. Hesselmeier-Hüttmann, D. Liu, R. Stöhr, W. Knolle, M. Ghezellou, J. Ul-Hassan, M. Schober, M. Bockstedte, G. Bian, A. Gali, V. Vorobyov, J. Wrachtrup, Single v_2 defect in 4H silicon carbide Schottky diode at low temperature, Nat. Commun. 16 (2025) http://dx.doi.org/10.1038/s41467-025-59647-9.
[30] D. Scheller, F. Hrunski, J. Schwarberg, W. Knolle, Ö. Soykal, P. Udvarhelyi, P. Narang, H. Weber, M. Hollendonner, R. Nagy, Quantum-enhanced electric field mapping within semiconductor devices, Phys. Rev. Appl. 24 (2025) 014036.
[31] P. Udvarhelyi, G. m. H. Thiering, N. Morioka, C. Babin, F. Kaiser, D. Lukin, T. Ohshima, J. Ul-Hassan, N.T. Son, J. Vučković, J. Wrachtrup, A. Gali, Vibronic states and their effect on the temperature and strain dependence of silicon-vacancy qubits in 4H-SiC, Phys. Rev. Appl. 13 (2020) 054017.
[32] J. Davidsson, R. Babar, D. Shafizadeh, I.G. Ivanov, V. Ivády, R. Armiento, I.A. Abrikosov, Exhaustive characterization of modified si vacancies in 4H-SiC, Nanophotonics 11 (2022) 4565–4580.
[33] V. Zalandauskas, R. Silkinis, L. Vines, L. Razinkovas, M.E. Bathen, Theory of the divacancy in 4H-SiC: Impact of jahn-teller effect on optical properties, 2024.